

Inline quality rating of multicrystalline wafers – Relevance, approach and performance of Al-BSF and PERC processes

Matthias Demant¹, Theresa Strauch¹, Kirsten Sunder², Oliver Anspach², Jonas Haunschild¹ & Stefan Rein¹

¹Fraunhofer Institute for Solar Energy Systems ISE, Freiburg; ²PV Crystalox Solar Silicon GmbH, Erfurt, Germany

ABSTRACT

With the transition of the cell structure from aluminium back-surface field (Al-BSF) to passivated emitter and rear cell (PERC), the efficiency of multicrystalline silicon (mc-Si) solar cells becomes more and more sensitive to variations in electrical material quality. Moreover, the variety of multicrystalline materials has increased with the introduction of high-performance multicrystalline (HPM) silicon. For these reasons, a reliable and verifiable assessment of the electrical material quality of multicrystalline wafers gains importance: to this end, a rating procedure based on photoluminescence (PL) imaging has been developed. The material quality is characterized by the distribution of crystallization-related defects, which are successfully correlated with the solar cell quality of PERC and Al-BSF solar cells. The applied image-processing and machine-learning techniques are outstandingly good because of their robustness, transparency and precision. This is demonstrated by an evaluation of the approach using a large database of wafers and cells from 72 bricks from nine different wafer manufacturers, which represent a broad spectrum of currently available materials. The quality prediction leads to mean absolute prediction errors of 2.2mV and 2.9mV for Al-BSF and PERC solar cells respectively, in a true blind test. The proposed wafer rating is of benefit to both wafer and cell manufacturers, and can be established during the pre-delivery inspection in wafer production, and the incoming inspection in solar cell production. While wafer manufacturers can improve material quality as a result of an immediate quality feedback after wafering, cell manufacturers can improve production yield because of an appropriate wafer selection.

Relevance and possibilities for a quality rating

The electrical quality of the wafer material has considerable impact on the achievable cell efficiency. Especially for passivated emitter and rear cells (PERC), solar cell efficiency is less limited by the surface recombination on the rear side, compared with solar cells with an aluminium back-surface field (Al-BSF); thus other factors gain importance. The quality of PERC solar cells is more sensitive to bulk recombination and hence to variations in the material quality. Since PERC cells are progressively replacing Al-BSF solar cells in mass production, an improved material quality and a reliable material selection are essential.

Recent developments of feedstock and the crystallization process have led to an improved class of material, the so-called ‘high-performance’ multicrystalline (HPM) Si [1]. Despite large differences in the price and quality of wafer materials, no specification in terms of the electrical material quality has yet been verified and established. The focus of this work is a reproducible quality description

of standard and HPM wafers based on photoluminescence (PL) imaging techniques [2].

“The establishment of a defect description requires a meaningful quantification of crystal defects and an evaluation of the rating capability for a broad set of materials.”

Feedstock and the crystallization process determine the types and distributions of defects. The quality of the feedstock can be quantified by the impurity grade of the granules. A more challenging task, however, is the characterization of material defects which form during the crystallization process and reduce charge-carrier lifetime. On the one hand, impurities from the coated crystallization crucible diffuse into the crystallized ingot; this leads to edge regions with increased metal contamination (e.g. Schubert et

al. [3] and Schindler et al. [4]). On the other hand, structural defects, such as grain boundaries and dislocations, form during the growth process. The novel concept of HPM reduces the generation and multiplication of dislocations. The different types of defect distribution have to be considered in a wafer rating.

PL imaging [2] already allows these structural defects and contaminated regions to be measured inline at the as-cut stage [5]. This technique’s applicability is evaluated in the ISE approach for a wide range of wafer and solar cell data from different manufacturers and crystallization processes. Physically relevant defect features are quantified by means of image-processing techniques to form the basis of a wafer characterization. The presented detection and quantification of crystal defects allows a more detailed wafer description than currently available approaches in industry. The classification itself is based on machine-learning techniques. For this purpose, a regression model is trained in order to predict the expected solar cell quality.

The establishment of a defect

description requires a meaningful quantification of crystal defects and an evaluation of the rating capability for a broad set of materials, including material from unknown manufacturers, which was not part of the training data for the model. This level of distinction was first encountered by Demant et al. [6] and is presented in this paper.

Existing approaches for quality rating

Structural defects and impurities lead to an increased recombination of charge carriers at the defect location; these recombination-active defects become visible in PL images through a reduced luminescence signal. Alternative methods for lifetime measurement are, for example, the quasi-steady-state photoconductance (QSSPC) approach [7], which averages the carrier lifetime over larger areas, and the microwave-detected photoconductance approach (MDP) [8], which allows spatially resolved lifetime maps. The focus in this paper will be on PL imaging, since the method permits a quick investigation of defect structures, with the highest spatial resolution in the range of $160\mu\text{m}/\text{pixel}$. Commercial inline PL systems with megapixel resolution have been reported (e.g. Chunduri [9]).

On surface-passivated samples, the measured PL intensity directly reflects the electrical quality of the wafer bulk (e.g. Michl et al. [10]). Although the measured PL intensity of an as-cut wafer does not directly reflect the electrical quality of the wafer bulk, the geometrical structure of the structural defects present is already completely visible at the as-cut stage. PL measurements are therefore well suited to a 100% inline control at the as-cut stage. Four representative samples with different defect signatures, along with the corresponding solar cell efficiencies, are illustrated in Fig. 1.

The defect structures determined in PL images of as-cut wafers correlate with solar cell performance [5,11,12]. Features for assessing material quality have been included in multivariate rating models [13–15]. This paper describes a multivariate, feature-based prediction approach that was published in greater detail by Demant et al. [6]. The richness of the underlying data set surpasses all recent investigations in this field. The data set allows different levels of difficulty in classification to be distinguished; in particular, the prediction of unknown manufacturers is necessary for a sound rating model created on the basis of a

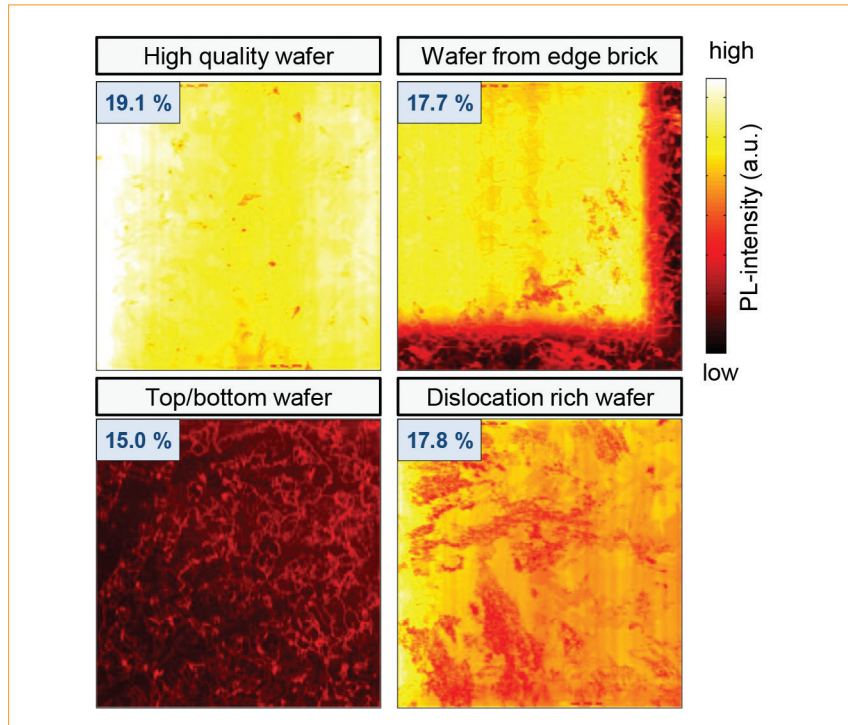


Figure 1. PL images of different bricks and brick positions, along with the conversion efficiencies of PERC cells manufactured from those wafers.

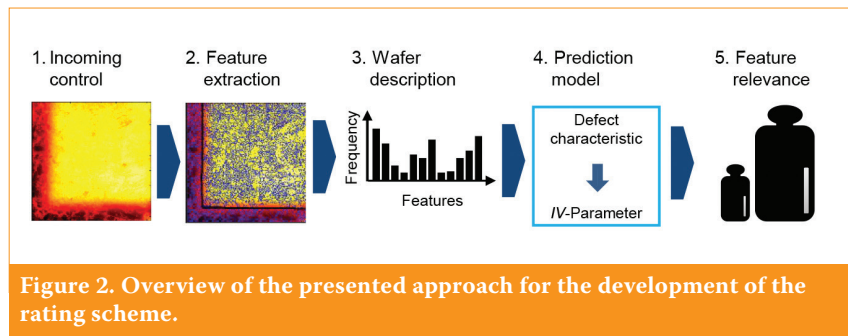


Figure 2. Overview of the presented approach for the development of the rating scheme.

powerful multivariate data analysis.

The impact of defect features on solar cell performance also shows a direct dependency on the solar cell process, for example via gettering during emitter diffusion [16]. Different types of structural defect have been distinguished in terms of their appearance and development during the cell process [17,18]. The local density of these structural defects may be connected to the development of different defect types [19]. In the approach presented in this paper, the issue is addressed by a quantification of the local defect density which is used to describe the wafer characteristics. Moreover, crystal defects inside and outside the contaminated regions are distinguished within the ISE approach, as a beneficial effect of crystal defects on the gettering behaviour in the contaminated regions has been shown by Bentzen & Holt [20]. The relevance of these features can be observed with the proposed classification model via a regularized form of multivariate regression.

Novel machine-learning-based approach for quality rating

Overview

The principal goal is to establish a prediction model to forecast the solar cell quality from PL images of as-cut wafers, and to identify the most relevant features for devising a rating of the material quality. The target parameter of the rating model is the open-circuit voltage V_{oc} , which strongly correlates with material quality and is quite robust with respect to process variations. The rating model is outlined in Fig. 2 and comprises the following steps:

- 1. Incoming control:** the wafer first passes an incoming control with inline PL imaging.
- 2. Feature extraction:** special image-processing techniques are applied in order to detect crystal defects, despite variations in contrast.

3. Wafer description: the defects are quantified within a defect characterization to describe the wafer.

4. Prediction model: the rating scheme is trained to predict the solar cell quality on the basis of the empirical data of the as-cut measurements and the corresponding cell performances. It is

essential to evaluate the quality of the model for unknown data.

5. Feature relevance: the prediction model enables the relevance of the features to be analysed; therefore, differences in the solar cell processes can be compared, and a deeper understanding can be gained by means of reference measurements.

Extraction of PL image features

Crystal defects and contaminated regions

The most important defect features are structural defects, such as dislocations and grain boundaries, which appear as dark, blurred line structures. Wafers with in-diffused impurities from the coated crystallization crucible exhibit large-area contaminated regions with reduced average PL intensities, which mostly appear on wafers from the top or bottom of the brick or on wafers taken from the edge or the corner bricks of an ingot.

As depicted in Fig. 3(a), the crystal defects appear as light structures within the contaminated regions; this reflects the gettering effect of the crystal defects in these regions. To allow a quantification of all structural defects, the structures of the PL images are extracted, as shown in Fig. 3(b). In a second step, all crystal defects are quantified according to the phase congruency model of edge detection [21], which leads to a contrast-invariant localization of crystal defects, shown in Fig. 3(c). The first defect feature, Feature 1, equals the area fraction of crystal defects (see Fig. 3(c)).

Since crystal defects are slightly blurred in the PL images, the defect structures are thinned. The second defect feature, Feature 2, quantifies the area fraction of

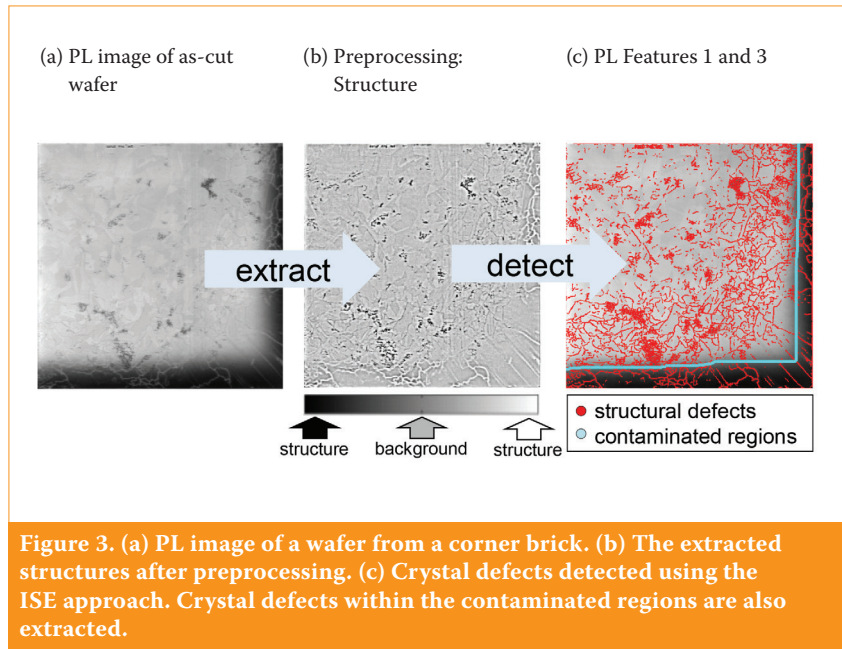


Figure 3. (a) PL image of a wafer from a corner brick. (b) The extracted structures after preprocessing. (c) Crystal defects detected using the ISE approach. Crystal defects within the contaminated regions are also extracted.

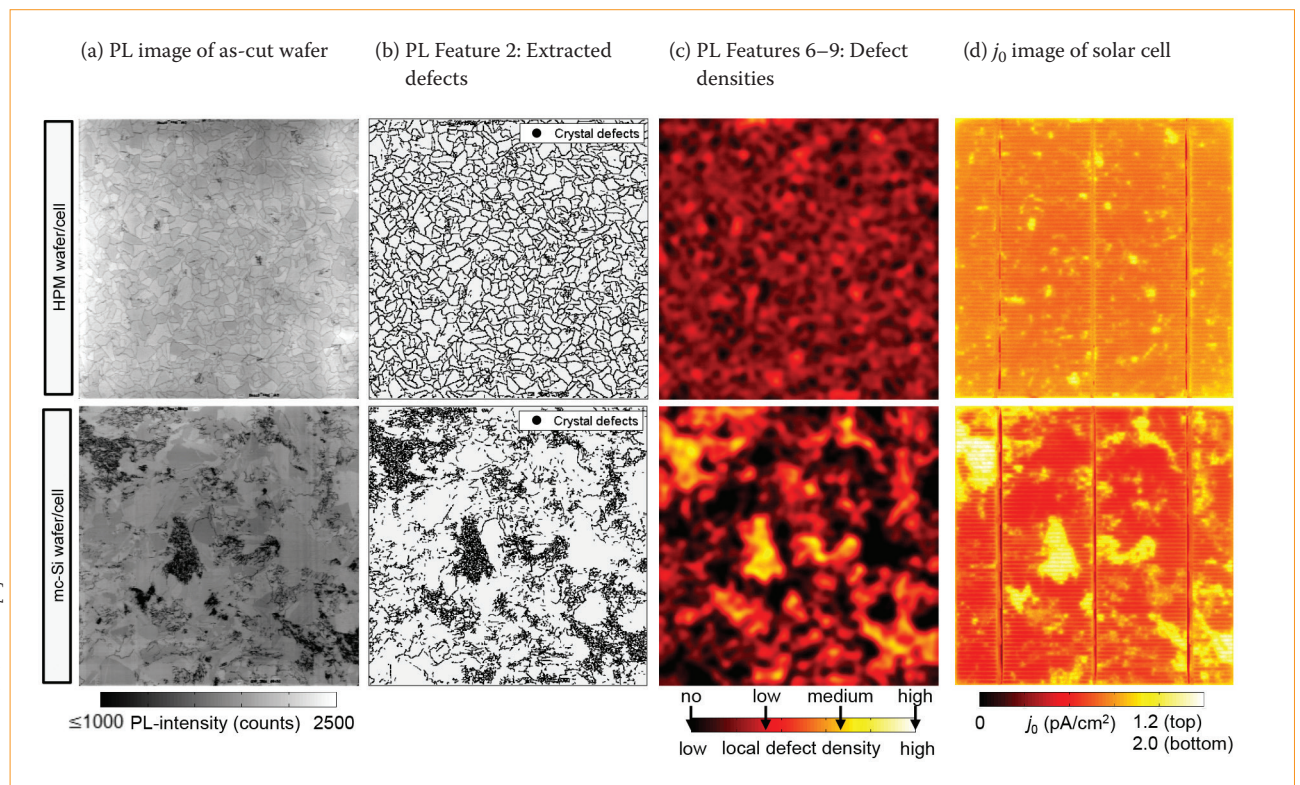


Figure 4. Appearance of crystal defects in a HPM Si wafer (top row) and a regular mc-Si wafer (bottom row). (a) PL images taken at the as-cut stage. (b) Extracted defects. (c) Corresponding local defect densities, revealing a difference between the materials – the HPM wafer (top) contains equally distributed defects, whereas the standard mc-Si wafer (bottom) contains dense dislocation clusters, as well as defect-free regions. These differences are quantified in the four parameters of the area fraction: no, low, medium and high local defect density. (d) The j_0 images of the solar cells are in good agreement with the features observed in the as-cut stage.

Source: Demant et al. [6].

thinned crystal defects (see Fig. 4(b)). The area fraction of the contaminated region, Feature 3, is also added to the ISE wafer description (see Fig. 3(c)); this is computed using basic image-processing techniques. The information about the contaminated regions allows the quantification of crystal defects in regions with low lifetime due to the contaminant's in-diffusion from the crucible (Feature 4), and distinguishes them from crystal defects within non-contaminated wafer areas (Feature 5). The differentiation is beneficial because defect clusters may act as gettering sites within contaminated regions [20]. To the best of the authors' knowledge, these features are not detected in most industrial algorithms, which frequently consider only two or three features.

Distribution of crystal defects and intensities

The distribution of crystal defects throughout the wafer plane also influences the solar cell quality, as simulated by Isenberg et al. [22]. These material differences are quantified by computing local defect densities by a Gaussian averaging. Regions with no, low, medium and high (Features 6 to 9; see Fig. 4(c)) local defect densities are distinguished.

With HPM, crystallization dislocations are avoided because of a large quantity of small grains with random grain boundaries. Regions of low defect densities are therefore observed in HPM wafers, whereas a large number of dense crystal defects, mostly dislocations, can be observed in standard mc-Si wafers, as shown in Fig. 4. The correlation of defect regions of medium or high dislocation density with the corresponding image region of the dark-saturation current density (j_0 images) confirms the relevance of these features. In addition, structural defect densities in contaminated regions and non-contaminated regions are quantified separately and added to the set of features (Features 10 to 17).

Further features are the average PL intensity (Feature 18), the doping normalized PL intensity (Feature 19), and the area fractions of regions with increasing levels of average PL intensity (Features 20 to 24; see Fig. 5). Finally, whether the wafer originates from the top/bottom region of the brick and shows completely inverted PL contrasts (Feature 25) is analysed.

Regression models

A challenge in multivariate data analysis is avoiding models that over-fit the training data and lead to a poor prediction quality of unknown samples. On the other hand, models of very low complexity may

not be capable of describing complex relationships, which leads to a bias in the data. The optimum model can be identified within a model-selection step using a validation set of data. According to Occam's razor, a simple prediction model should be preferred to more complex models, provided it can explain the given relationship. Three models with different model complexities were therefore analysed.

“A challenge in multivariate data analysis is avoiding models that over-fit the training data and lead to a poor prediction quality of unknown samples.”

The first method is a support vector regression (SVR): this is a supervised machine-learning technique, which can predict non-linear relationships. A regression model is trained to rate an input feature vector $\vec{x} = (x_1, \dots, x_p)$

according to a quality parameter y . The algorithm primarily learns the mapping from features to the output (open-circuit voltage) from training data. Vapnik's ε -SV regression model [23] is trained with a radial basis kernel. The meta-parameters ε and c are determined via a grid search on a validation subset of the data.

Second, a multilinear prediction model is used to predict the solar cell quality y_i on the basis of the set of features $x_{i,j}$ with $j \in \{0, \dots, p\}$ for sample $i \in \{0, \dots, n\}$. More precisely, the goal is to determine the coefficients β_k with $k \in \{0, \dots, p\}$ that minimize the prediction error for the training set with n elements according to

$$\vec{\beta} = \operatorname{argmin}_{\vec{\beta}} \left\{ \frac{1}{2n} \sum_{i=1}^n (y_i - \beta_0 - \sum_{j=1}^p x_{i,j} \beta_j)^2 + \lambda P(\vec{\beta}) \right\} \quad (1)$$

At this stage, Occam's razor is followed by applying a regularized form of regression – the elastic-net algorithm [24]. The number of coefficients is penalized according to a penalty function $P(\vec{\beta})$ with a regularization term λ ; with a lower value of λ a more complex model is

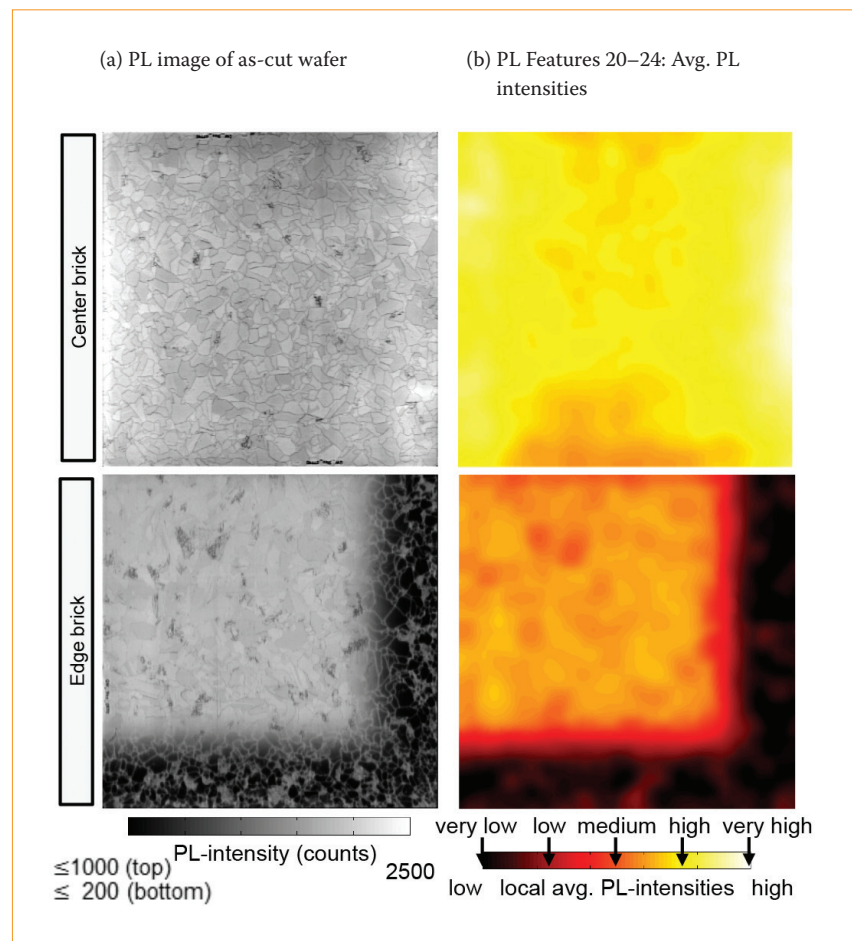


Figure 5. Examples of (a) PL images and (b) corresponding local average PL intensities of wafers from an HPM crystallization (top row) and a regular multicrystalline crystallization (bottom row). The local average PL intensities are quantified in the five parameters of the area fraction: very low, low, medium, high and very high average PL intensity.

Source: Demant et al. [6].

allowed. The penalty function can be the ℓ_2 norm ($P(\beta) = \|\beta\|_2$) or the ℓ_1 norm ($P(\beta) = \|\beta\|_1$) or a value in between, as proposed in the elastic-net approach. In the last two cases, fewer active features are preferred to solutions with many active features. The most robust model is identified within the model selection step. Finally, the predicted solar cell quality \hat{y} is given by $\hat{y} = \hat{\beta}(\bar{x}^T, 1)^T$.

The third method is a simple two-feature approach. The two features quantify dislocation clusters x_{clust} and the area of contaminated regions x_{cont} ; these are extracted on the basis of morphological operations. The calculation of the expected quality \hat{y} is based on the maximum expected solar cell quality q_{max} , where $q_{\text{max}} = V_{\text{oc,max}}$, according to

$$\hat{y} = q_{\text{max}} - \beta_{\text{clust}} x_{\text{clust}} - \beta_{\text{cont}} (x_{\text{cont}} - \beta_{\text{fix}}) \quad (2)$$

with coefficients β_{clust} , β_{cont} and β_{fix} . The parameter β_{fix} describes an expected positive gettering effect on contaminated edge regions, similar to the approach of Birkmann et al. [12].

Experimental approach for the qualification of a wafer rating

Materials and experimental approach

A large set of about 7,500 wafers from nine manufacturers was investigated using two different production processes, as shown in Fig. 6. Most

of the material (7,000 wafers) was selected from wafer sets with known ingot and brick positions provided by nine different manufacturers. To create a wafer set which represents the full spectrum of possible defect constellations, the wafers were systematically sampled from different brick positions of 72 bricks, the bricks being selected from 16 ingots from different ingot positions within the crystallization crucible. Additional material was sampled from 27 boxes from two manufacturers.

In the as-cut state, all wafers were subjected to an initial incoming control using commercially available inline measurement equipment (including conductivity and thickness measurements and micro-crack detection) and an inline PL system. The rating model is developed using this comprehensive data set, collected in the incoming control operation.

The wafer material was split into two sets for use in two different solar cell processes, one with 6,450 wafers and one with 1,050 wafers. The batch with 6,450 wafers was used to fabricate PERC solar cells in an industrial cell production line; the other batch, with 1,050 wafers, was used to create Al-BSF solar cells with screen-printed and fired, Ag and Al front- and rear-side metal contacts in the PV-TEC research line [25]. In both cases, neighbouring wafers were processed to ensure comparability of the rating. Furthermore, a representative subset of 47 bricks was

selected for the smaller batch (the Al-BSF process) from all 72 bricks considered within the PERC process.

The two material classes HPM and mc-Si were distinguished qualitatively according to their grain structure. In the outgoing quality control operation, the current–voltage (I – V) characteristics were measured under standard test conditions. To allow a spatially resolved analysis of the defect structure in the final cells, the images of the dark-saturation current density j_0 were generated for selected samples by C-DCR imaging accordant with Glatthar et al. [26].

Evaluation set-up

A set of characteristic PL features is extracted using the data of the incoming control. The doping concentration (Feature 26), which was determined from inductive conductivity measurements [27], and the total thickness variation (Feature 27), are also added to the set of features. The proposed machine-learning techniques are applied and compared with respect to the prediction accuracy of the V_{oc} . The mean absolute error (MAE) between predicted and measured V_{oc} is selected as the quality metric. Furthermore, the root mean square error (RMS) and Pearson correlation coefficient (Corr) are determined.

In general, the application of powerful machine-learning techniques requires the evaluation of ‘unknown’ data; therefore, the data sets are split into disjoint training and testing sets for a valid evaluation of the prediction model. Frequently, a random selection of data is utilized. An advanced randomization can be used with the k -fold cross validation (e.g. Bishop [28]); by randomly splitting the data into k folds, all the data can be analysed. One of the k folds is iteratively predicted with a model trained by the remaining $(k-1)$ folds.

The challenge of a prediction model to make an accurate prediction increases with a decreasing degree of similarity between training and test sets. The analysis of data from unknown manufacturers, which represents the most challenging case, is considered in the second evaluation in this work. Iteratively, the data set of each manufacturer is selected as a test set and evaluated with a rating model trained on the data set containing all remaining manufacturers; each classification model is evaluated for these training/testing configurations. The elastic-net regression returns the most relevant features for both solar cell processes, which are then compared with respect to the most-influencing material

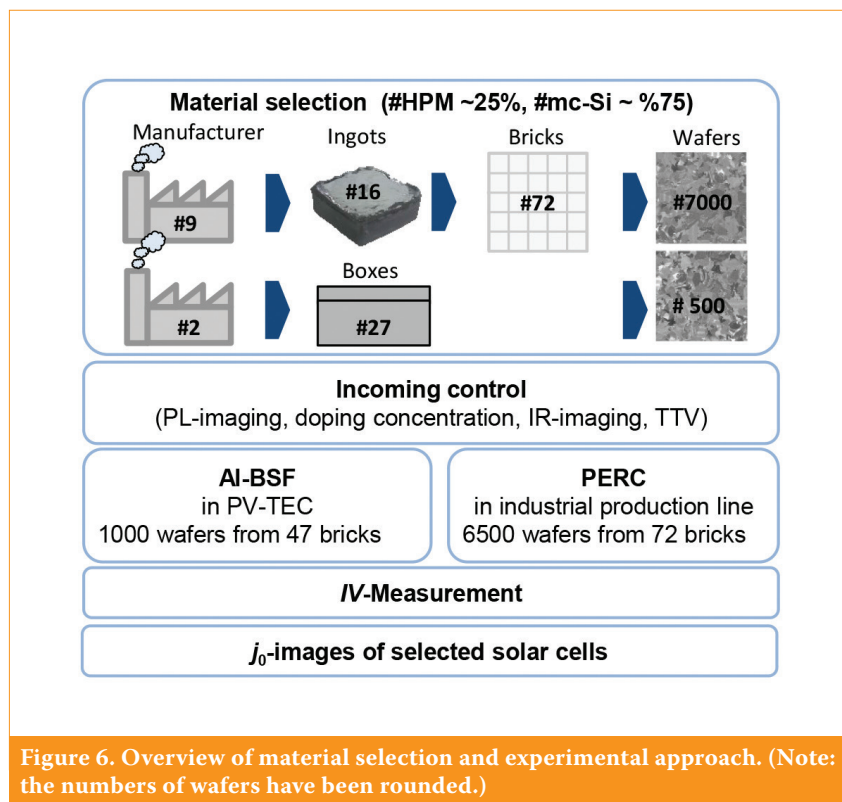


Figure 6. Overview of material selection and experimental approach. (Note: the numbers of wafers have been rounded.)

features. Finally, the appearance of these relevant features in both processes and material classes (HPM and mc-Si) are considered within a more detailed comparison based on the j_0 images of the final cells.

Quality of the different rating approaches

The PL images were analysed on the basis of the algorithm described in detail by Demant et al. [6]. The wafers were processed into solar cells, with V_{oc} values in the range 600–630mV for the Al-BSF process and 610–650mV for the PERC process (neglecting outliers). The broad V_{oc} range directly reflects the broad material spectrum. As expected, the PERC process reacts more sensitively than the Al-BSF process to the variations in material quality. The

main evaluation results are listed in Table 1 and discussed next.

The prediction of V_{oc} using a random selection of data ('Evaluation 1') yields very good results for the Al-BSF process, with MAE values of 1.3mV, 2.0mV and 2.1mV for the SVR, elastic-net and two-feature approaches respectively. The evaluation of the prediction quality of the set of PERC data, however, shows larger differences between the models. The qualities of the rating models are nevertheless ordered the same, with SVR achieving the smallest error (MAE=1.4mV). The elastic-net approach yields a slight increase in prediction error (MAE=2.5mV), whereas the simple two-feature model completely fails to predict the solar cell quality within an industrial PERC process (MAE=6.9mV). The complex SVR therefore performs best for

randomly selected data, regardless of the solar cell process. The high prediction quality reflects the quality of the approach but is also due to the remaining similarity between the training and test sets. Even for a random selection, however, the training and test sets do not include neighbouring wafers within the data set used.

In the case of forecasting material from an unknown manufacturer, this similarity is completely eliminated. The results in Fig. 7 show an example for the prediction of wafers from two unknown manufacturers ('Evaluation 2a') with HPM and standard mc-Si material for the Al-BSF and PERC processes. For the Al-BSF process, the elastic-net algorithm yields the best performance (MAE=1.8mV), followed by the SVR method (MAE=2.0mV) and the two-feature approach (MAE=2.1mV), with

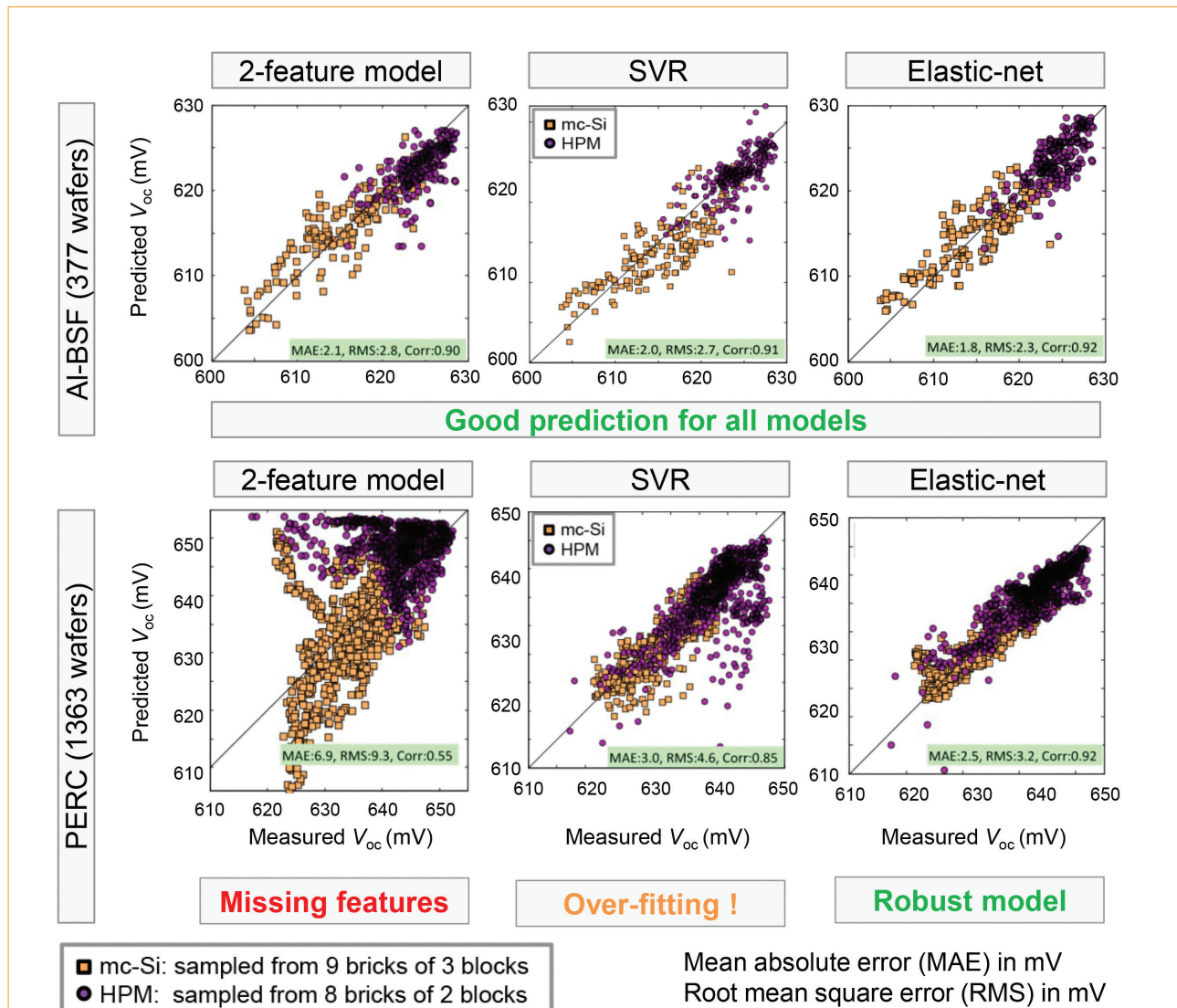


Figure 7. Prediction results for wafers from two unknown manufacturers (Evaluation 2a) for both solar cell processes, PERC and Al-BSE, obtained using the simple two-feature (left), complex SVR (middle) and elastic-net (right) approaches. The Al-BSF data prediction (top row) shows high correlations for all three prediction models. The PERC data prediction (bottom row) can be achieved with the SVR and elastic-net approaches, while the two-feature method fails completely.

Model	Solar cell process	Two-feature model [mV]	Support vector regression [mV]	Elastic-net algorithm [mV]
Complexity		Simple	Robust and non-linear	Linear, with optimized features
Evaluation 1: Random test set selection with fivefold cross-validation (MAE)	AI-BSF	2.1	1.3	2.0
	PERC	6.9	1.4	2.5
Evaluation 2a: Prediction of materials from two unknown manufacturers with HPM and standard wafers (MAE, cf. Fig. 7)	AI-BSF	2.1	2.0	1.8
	PERC	6.9	3.0	2.5
Evaluation 2b: Systematic prediction of wafers from each manufacturer, on the basis of training with wafers from the remaining manufacturers (overall MAE)	AI-BSF	2.1	2.2	2.2
	PERC	5.6	3.5	2.9

Table 1. Overview of the prediction quality of the investigated regression models for different training and test configurations and solar cell data. Prediction qualities are quantified by the mean absolute error (MAE) of the prediction. (The term ‘unknown manufacturer’ denotes that no material from this manufacturer was represented in the training data.)

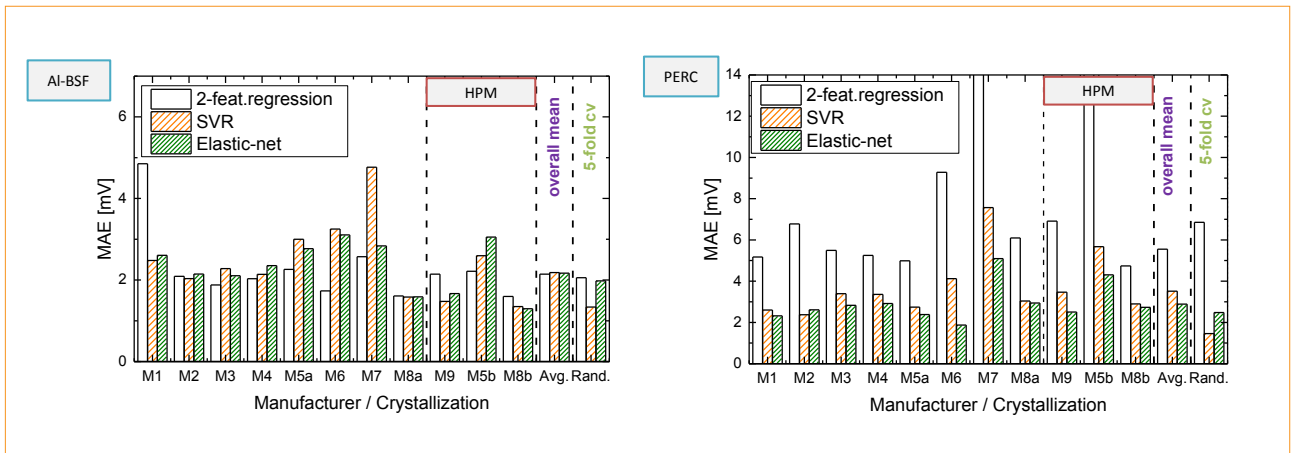


Figure 8. Prediction quality of material from an unknown manufacturer. The MAE is given for each manufacturer and is based on models trained using the remaining materials. The last two columns indicate the overall mean prediction result (‘Avg.’) and the prediction result on randomly selected test data (‘Rand.’). The elastic-net approach demonstrates the lowest overall MAE for the PERC prediction data.

slightly higher prediction errors. This ranking is even more distinct for the PERC prediction: while the elastic-net approach produces low prediction errors (MAE=2.5mV), the prediction errors are higher for the SVR model (MAE=3.0mV), and the simple two-feature-model fails completely (MAE=6.9mV).

In addition, for unknown material, the prediction quality of the three approaches was systematically evaluated (‘Evaluation 2b’): the material from each of the manufacturers was rated consecutively with the three models, each of the models being trained using the material from all the other manufacturers. The results are presented in Fig. 8, which shows the MAE values of the prediction for each manufacturer and all three prediction models; the overall MAE summarizes the result for all manufacturers. The classification accuracy for the AI-BSF process is high with all three approaches.

As regards the PERC process, it can be seen in Fig. 8 that the simple two-feature approach mostly fails for all the different

manufacturers (overall MAE=5.6mV). The prediction quality for SVR is also poor (overall MAE=3.5mV), which may be connected to an overfitting to the training data. In this most challenging task the robust elastic-net algorithm performs best (overall MAE=2.9mV); this can be interpreted as a very good result, considering the broad distribution of V_{oc} values ranging from 40mV and above, and the pure process- and measurement-related V_{oc} variations in the range of ~2mV.

Identification of relevant features

The applied elastic-net regression model allows the V_{oc} to be predicted and the relevance of the features to be simultaneously selected and rated. The model selection identifies a robust model with the most relevant features only. For normalized features, the coefficients of the linear regression model indicate the importance of the parameters.

The most important features for the

prediction of samples from both types of solar cell are the area fraction of thinned dislocations (Feature 2), and the area fraction of regions with low (Feature 7) and medium (Feature 8) local defect densities. Feature 2 represents dislocations or grain boundaries, which are thinned to their centres. As expected, the predicted solar cell quality decreases with the number of thinned structural defects and clusters of structural defects (Feature 8). On the other hand, it increases with the number of sparse structural defects (Feature 7), such as grain boundaries, which represent most structural defects identified in HPM wafers (see Fig. 4). These structures are less critical than dislocation clusters. For both types of solar cell, the distribution of PL structures and PL intensities plays an important role. The doping concentration was also considered to be a relevant feature in the rating model.

For PERC cells the second most important feature is different from that in the AI-BSF results: it quantifies instead the area fraction of regions

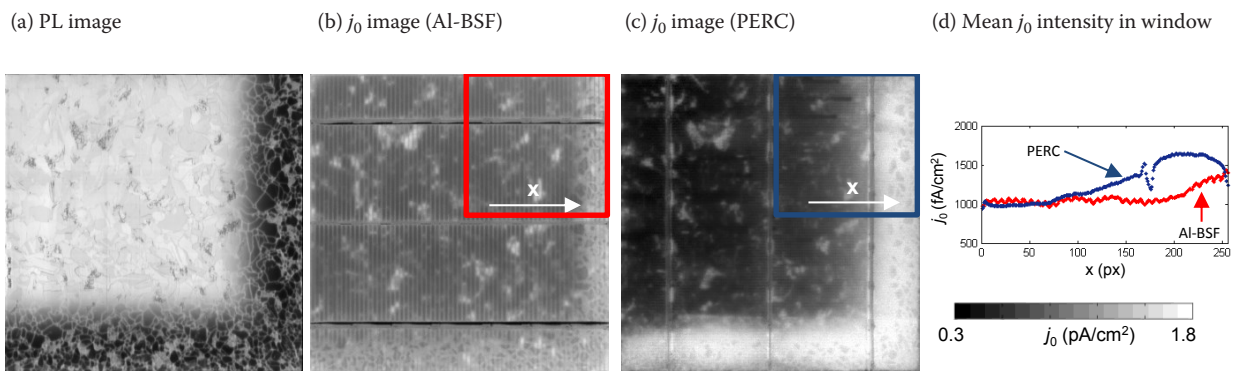


Figure 9. (a) PL image of a wafer from a corner brick. (b) The j_0 image obtained from the C-DCR method on an Al-BSF solar cell manufactured from the investigated wafer and a neighbouring wafer. (c) Corresponding j_0 image for a PERC cell. (d) Mean intensity profiles and j_0 values near the edges of the wafer, showing the effects of the diffusion processes.

with very low luminescence intensity (Feature 20) and has a strong negative impact on cell performance. According to the authors' empirical evaluation, the area fraction of very low luminescence intensity replaces the quantification of contaminated regions (Feature 3).

The differences between PERC and Al-BSF cells were investigated by comparing the images of dark-saturation current of two neighbouring wafers from a corner brick. The contaminated regions are visible in the PL image shown in Fig. 9(a). The contrast between the j_0 value in the contaminated regions and the non-contaminated regions is larger for PERC cells than for Al-BSF cells. This advantage of the Al-BSF process results from: 1) an enhanced phosphorus gettering during the two-sided emitter diffusion (which is reduced in the PERC process because of a one-sided emitter diffusion); and 2) the full-area aluminium gettering during rear-side contact formation (which no longer occurs in the PERC process because of the local contacting of the passivated rear side).

Conclusion and outlook

A classification scheme has been developed to simultaneously predict the solar cell quality of standard mc-Si and HPM wafers. The development was based on a representative set of 7,500 industrially available wafers from 72 bricks and nine manufacturers, which were intensively characterized in the as-cut state in an incoming inspection and then processed into solar cells using an Al-BSF and a PERC method.

“The results demonstrate the quality of the proposed elastic-net approach.”

The quantification of the defects that showed up in the PL images was improved by means of robust image-processing algorithms. Using regularized regression (elastic-net approach), the prediction of the open-circuit voltage for standard mc-Si manufacturers yielded average MAEs of 2.2mV for the Al-BSF solar cell process and 2.9mV for the PERC one. For an industrial PERC process, the prediction of the quality for unknown wafer manufacturers was slightly less accurate using the SVR approach (MAE=3.5mV), but completely failed using the simple two-feature approach (MAE=5.6mV). The results demonstrate the quality of the proposed elastic-net approach.

Most of the structural defects in HPM can be traced back to grain boundaries, which are quantified as regions with low local defect density and which marginally affect cell quality. Thus a rating scheme has to differentiate between different levels of defect density in order to rate both types of material under investigation. Different feature weights are also deemed necessary for Al-BSF and PERC solar cells.

In follow-up investigations, higher-order input parameters will be analysed. A modelling of relevant features as proposed by Demant et al. [29] by considering spatially resolved quality data (e.g. Glatthaar et al. [26]) can also be used to further refine the rating scheme. Moreover, advanced image-processing techniques have been developed at ISE to analyse the crystallization process in more detail using PL images of as-cut wafers; the extracted parameters allow the defect development to be rated during crystallization. The application of new computer-vision technologies, such as the so-called ‘deep learning’;

can further boost the material rating method. To implement such promising and data-intensive approaches, strong cooperation between industry and research will be necessary.

Acknowledgements

This work was supported by the German Ministry for Education and Research (BMBF) under the framework of the ‘Q-Wafer’ project (03SF0409).

References

- [1] Lan, C.W. et al. 2012, “Grain control in directional solidification of photovoltaicsilicon”, *J. Cryst. Growth*, Vol. 360, pp. 68–75.
- [2] Trupke, T. et al. 2006, “Photoluminescence imaging of silicon wafers”, *Appl. Phys. Lett.*, Vol. 89, pp. 1–3.
- [3] Schubert, M.C. et al. 2013, “Impact of impurities from crucible and coating on mc-silicon quality – The example of iron and cobalt”, *IEEE J. Photovolt.*, Vol. 3, pp. 1250–1258.
- [4] Schindler, F. et al. 2014, “Solar cell efficiency losses due to impurities from the crucible in multicrystalline silicon”, *IEEE J. Photovolt.*, Vol. 4, pp. 122–129.
- [5] Haunschild, J. et al. 2010, “Quality control of as-cut multicrystalline silicon wafers using photoluminescenceimagingforsolar cell production”, *Sol. Energy Mater. Sol. Cells*, Vol. 94, pp. 2007–2012.
- [6] Demant, M. et al. 2015, “Inline quality rating of multi-crystalline wafers basedonphotoluminescenceimages”, *Prog. Photovoltaics Res. Appl.*, doi: 10.1002/ppp.2706.
- [7] Sinton, R.A., Cuevas, A. & Stuckings, M. 1996, “Quasi-steady-state photoconductance, a new method for solar cell material and device characterization”, *Proc. 25th IEEE*

- PVSC, Washington DC, USA, pp. 457–460.
- [8] Dornich, K. et al. 2013, "Fast, high resolution, inline contactless electrical semiconductor characterization for photovoltaic applications by microwave detected photoconductivity", *Mater. Sci. Eng. B*, Vol. 178, pp. 676–681.
- [9] Chunduri, S.K. 2011, "Market survey on luminescence imaging systems and cameras", *Photon International*, Vol. 1, pp. 158–193.
- [10] Michl, B. et al. 2012, "Efficiency limiting bulk recombination in multicrystalline silicon solar cells", *Sol. Energy Mater. Sol. Cells*, Vol. 98, pp. 441–447.
- [11] Nagel, H. et al. 2010, "Luminescence imaging – a key metrology for crystalline silicon PV", *Proc. 20th Worksh. Cryst. Si. Sol. Cells & Mod.*, Breckenridge, Colorado, USA.
- [12] Birkmann, B. et al. 2011, "Analysis of multicrystalline wafers originating from corner and edge bricks and forecast of cell properties", *Proc. 26th EU PVSEC*, Hamburg, Germany, pp. 1–4.
- [13] Demant, M. et al. 2010, "Analysis of luminescence images applying pattern recognition techniques", *Proc. 25th EU PVSEC*, Valencia, Spain, pp. 1078–1082.
- [14] McMillan, W. et al. 2010, "In-line monitoring of electrical wafer quality using photoluminescence imaging", *Proc. 25th EU PVSEC*, Valencia, Spain, pp. 1346–1351.
- [15] Demant, M. et al. 2013, "Evaluation and improvement of a feature-based classification framework to rate the quality of multicrystalline silicon wafers", *Proc. 28th EU PVSEC*, Paris, France, pp. 1650–1654.
- [16] Glatthaar, M. et al. 2010, "Luminescence imaging for quantitative solar cell material and process characterization", *Proc. 25th EU PVSEC*, Valencia, Spain, pp. 1825–1827.
- [17] Bakowskie, R. et al. 2011, "Comparison of recombination active defects in multicrystalline silicon by means of photoluminescence imaging and reverse biased electroluminescence", *Proc. 26th EU PVSEC*, Hamburg, Germany, pp. 1839–1842.
- [18] Lausch, D. & Hagendorf, C. 2015, "Influence of different types of recombination active defects on the integral electrical properties of multicrystalline silicon solar cells", *J. Sol. Energy*, Vol. 2015, pp. 1–9.
- [19] Johnston, S. et al. 2012, "Comparison of photoluminescence imaging on starting multi-crystalline silicon wafers to finished cell performance", *Proc. 38th IEEE PVSC*, Austin, Texas, USA, pp. 2161–2166.
- [20] Bentzen, A. & Holt, A. 2009, "Overview of phosphorus diffusion and gettering in multicrystalline silicon", *Mater. Sci. Eng. B*, Vol. 159–160, pp. 228–234.
- [21] Kovesi, P. 2003, "Phase congruency detects corners and edges", *Austral. Patt. Recog. Soc. Conf.: DICTA 2003*, Sydney, Australia, pp. 309–318.
- [22] Isenberg, J. et al. 2003, "Imaging method for laterally resolved measurement of minority carrier densities and lifetimes: Measurement principle and first applications", *J. Appl. Phys.*, Vol. 93, pp. 4268–4275.
- [23] Vapnik, V. 1995, *The Nature of Statistical Learning Theory*. New York: Springer.
- [24] Hastie, T. et al. 2009, "Linear methods for regression", in *The Elements of Statistical Learning*, 2nd edn. New York: Springer, pp. 43–100.
- [25] Biro, D. et al. 2009, "PV-TEC: Retrospection to the three years of operation of a production oriented research platform", *Proc. 24th EU PVSEC*, Hamburg, Germany, pp. 1901–1905.
- [26] Glatthaar, M. et al. 2010, "Spatially resolved determination of dark saturation current and series resistance of silicon solar cells", *physica status solidi (RRL)*, Vol. 4, pp. 13–15.
- [27] Spitz, M., Belledin, U. & Rein, S. 2007, "Fast inductive inline measurement of the emitter sheet resistance in industrial solar cell fabrication", *Proc. 22nd EU PVSEC*, Milan, Italy, pp. 47–50.
- [28] Bishop, C.M. 2006, *Pattern Recognition and Machine Learning*. New York: Springer.
- [29] Demant, M. et al. 2012, "Modelling of physically relevant features in photoluminescence images", *Energy Procedia*, Vol. 27, pp. 247–252.

About the Authors



Matthias Demant studied computer science at the University of Freiburg, Germany. Since 2009 he has been a researcher at Fraunhofer ISE. He is currently working on his Ph.D., which involves the inline characterization of wafers and solar cells by means of pattern-recognition techniques.



Theresa Strauch received her diploma degree in mathematics from the University of Freiburg in 2012. Since then she has been

working at Fraunhofer ISE on image processing with applications in wafer characterization. For her Ph.D. thesis, she is focusing on grain structure and dislocation development in silicon ingots.



Kirsten Sunder completed her physics diploma, with a focus on material physics, at the University of Münster, Germany. She continued working at the Institute of Materials Physics and received her Ph.D. for her work on network former diffusion in silicate glasses. Since 2011 she has been working as a scientist at PV Crystalox Solar Silicon GmbH in Erfurt, Germany.



Oliver Anspach studied geology at the Universities of Jena and Edinburgh, and received his Ph.D. from the Otto-Schott Institute for Glass Chemistry at the University of Jena. Since 2005 he has been working for PV Crystalox Solar PLC, and for the past eight years he has been responsible for R&D in the field of multiwire sawing.



Jonas Haunschild leads the inline wafer analysis team at Fraunhofer ISE. He studied physics at the Philipp University of Marburg and received a diploma degree in 2007, followed by his Ph.D. in 2012 for his work on luminescence-based methods for quality control in industrial solar cell production.



Stefan Rein is head of the inline measurement techniques and quality assurance group at Fraunhofer ISE, which focuses on metrology, production control, solar cell simulation and new silicon materials. He studied physics at the University of Freiburg and received his Ph.D. in 2004 for his work on lifetime spectroscopy for defect characterization in silicon.

Enquiries

Matthias Demant
PV Production Technology and Quality Assurance Dept.
Fraunhofer Institute for Solar Energy Systems ISE
Heidenhofstraße 2, 79110 Freiburg
Germany

Tel: +49 (0) 761/4588-5651

Email: matthias.demant@ise.fraunhofer.de